AD-A210 307

(2)

AFOSR-TR- 89-0992

INFLUENCE OF MICROSTRUCTURE AND MICRODAMAGE PROCESSES ON FRACTURE AT HIGH LOADING RATES

June 1989

Final Report

By: J. H. Giovanola, R. W. Klopp, J. W. Simons, T. Kobayashi, and D. A. Shockey

Prepared for:
AIR FORCE OFFICE OF SCIENTIFIC RESEARCH
AFOSR/NE, Bldg. 410
Bolling Air Force Base
Washington, DC 20332

Attn: Dr. Alan Rosenstein

Contract AFOSR/F49620-86-K-0010

SRI Project PYU-1750

SRI International
333 Ravenswood Avenue
Menlo Park, California 94025-3493
(415) 326-6200
TWX: 910-373-2046
Telex: 334486

SRI International

UNCLASSIFIED

SECURITY CLASSIFICATION OF THIS PAGE

REPORT DOCUMENTATION PAGE

1a. REPORT SECURITY CLASSIFICATION: Unclassified	1b. RESTRICTIVE MARKINGS
2a. SECURITY CLASSIFICATION AUTHORITY: N/A	3. DISTRIBUTION/AVAILABILITY OF REPORT: Approved for public release; distribution unlimited.
2b. DECLASSIFICATION/DOWNGRADING SCHEDULE: N/A	
4. PERFORMING ORGANIZATION REPORT NUMBER(S)	5. MONITORING ORGANIZATION REPORT NUMBER(S): AFOSR-TR- 89-0992
6a. NAME OF PERFORMING ORGANIZATION: SRI International; 6b. OFFICE SYMBOL (If applicable)	7a. NAME OF MONITORING ORGANIZATION: Air Force Office of Scientific Research
6c. ADDRESS (City, State, and ZIP Code): 333 Ravenswood Avenue, Menlo Park, CA 94025-3493	7b. ADDRESS (City, State, and ZIP Code): AFOSR/NE, Bldg. 410, Bolling Air Force Base, Washington, DC 20332
8a. NAME OF FUNDING/SPONSORING ORGANIZATION: AFOSR; 8b. OFFICE SYMBOL (If applicable): NE	9. PROCUREMENT INSTRUMENT IDENTIFICATION NUMBER: ~~AFOSR~~/F49620-86-K-0010
8c. ADDRESS (City, State, and ZIP Code): Bldg. 410, Bolling AFB, DC 20332-6448	10. SOURCE OF FUNDING NUMBERS: PROGRAM ELEMENT NO. 61102-F; PROJECT NO. 2306; TASK NO. A1; WORK UNIT ACCESSION NO.

11. TITLE (Include Security Classification): INFLUENCE OF MICROSTRUCTURE AND MICRODAMAGE PROCESSES ON FRACTURE AT HIGH LOADING RATES

12. PERSONAL AUTHOR(S): Giovanola, J. H., Klopp, R. W., Simons, J. W., Kobayashi, T., and Shockey, D. A.

13a. TYPE OF REPORT	13b. TIME COVERED	14. DATE OF REPORT (Year, Month, Day)	15. PAGE COUNT
Final	FROM 860201 TO 880930	890626	

16. SUPPLEMENTARY NOTATION

17. COSATI CODES FIELD	GROUP	SUB-GROUP
11	06	02
20	11	

18. SUBJECT TERMS (Continue on reverse if necessary and identify by block number): titanium alloy, microstructures, fracture behavior, loading rate, microdamage, microdeformation, microstructure models

19. ABSTRACT (Continue on reverse if necessary and identify by block number)

The objectives of this three-year program were to establish how microstructure and loading rate influence the fracture behavior of Ti-10V-2Fe-3Al, a promising advanced titanium alloy increasingly used in aircraft structural components, and to relate the macroscopic fracture toughness results to microdeformation and microdamage processes with a view toward developing microstructurally based fracture models. Such models are desirable to develop compositions and processing conditions resulting in optimum mechanical properties.

Three microstructures of Ti-10V-2Fe-3Al with comparable strength and grain size but different amounts of primary alpha phase (α_p) were investigated. For a given grain size distribution (50-300 μm), strength level (1180 ± 100 MPa), and loading rate, variations in solution treatment temperature to vary the α_p content (0% to approximately 40%) resulted in only a small increase in initiation fracture toughness (from 56 to 63 MPa$\sqrt{m}$ for static loading and from 62 to 75 MPa$\sqrt{m}$ for dynamic loading). Varying the loading rate from 2×10^{-1} to 1.4×10^{6} MPa$\sqrt{m}$s^{-1} also has only a small effect on initiation fracture toughness.

20. DISTRIBUTION/AVAILABILITY OF ABSTRACT: [X] UNCLASSIFIED/UNLIMITED [ ] SAME AS RPT. [ ] DTIC USERS	21. ABSTRACT SECURITY CLASSIFICATION: UNCLASSIFIED
22a. NAME OF RESPONSIBLE INDIVIDUAL: DR ALAN ROSENSTEIN	22b. TELEPHONE (Include Area Code): (202) 767-4933; 22c. OFFICE SYMBOL: NE

DD FORM 1473, 84 MAR — 83 APR edition may be used until exhausted. All other editions are obsolete.

SECURITY CLASSIFICATION OF THIS PAGE

UNCLASSIFIED

18. SUBJECT TERMS (Continued)

fractography
fracture toughness
crack propagation
FRASTA

19. ABSTRACT (Continued)

In contrast, dynamic crack propagation toughness is strongly affected by α_p content. The 40% α_p microstructure has the highest propagation toughness ($K_{ID} \approx 120$ MPa$\sqrt{m}$), the 12% α_p microstructure has a somewhat lower toughness ($K_{ID} \approx 100$ MPa$\sqrt{m}$), and the 0% α_p microstructure has significantly lower toughness ($K_{ID} \approx 65$ MPa$\sqrt{m}$). The dynamic propagation toughness for the α_p-containing microstructures is up to 70% higher than the dynamic initiation toughness. The increases in propagation toughness above the dynamic initiation toughness are due to a resistance curve effect associated with the formation of small shear lips during crack extension. The present results suggest that the tendency to form shear lips is a sensitive function of the microstructural condition. In the range of crack velocities investigated (50 to 450 m/s), dynamic propagation toughness was independent of crack velocity.

Scanning electron microscopy and fractography using fracture reconstruction applying surface topography analysis (FRASTA) showed that the proportion of intergranular failure decreases with increasing α_p content, that localized deformation within grains or at grain boundaries is a dominant mechanism in microdamage initiation, and that microcracking ahead of the main crack front and often normal to the main crack plane plays an important role in the crack extension mechanism. High loading rates enhance the tendency for slip localization, leading to the formation of long tubular cavities, which markedly change the fracture surface morphology of all investigated microstructures. Crack tip opening displacement values obtained with FRASTA confirm the initiation toughness results.

A proposed microstructural damage model is outlined, and recommendations for further studies are presented.

SUMMARY

The objectives of this three-year program were to establish how microstructure and loading rate influence the fracture behavior of Ti-10V-2Fe-3Al, a promising advanced titanium alloy increasingly used in aircraft structural components, and to relate the macroscopic fracture toughness results to microdeformation and microdamage processes with a view toward developing microstructurally based fracture models. Such models are desirable to develop compositions and processing conditions resulting in optimum mechanical properties.

Three microstructures of Ti-10V-2Fe-3Al with comparable strength and grain size but different amounts of primary alpha phase (α_p) were investigated. For a given grain size distribution (50-300 μm), strength level (1180 ± 100 MPa), and loading rate, variations in solution treatment temperature to vary the α_p content (0% to approximately 40%) resulted in only a small increase in initiation fracture toughness (from 56 to 63 MPa$\sqrt{m}$ for static loading and from 62 to 75 MPa$\sqrt{m}$ for dynamic loading). Varying the loading rate from 2×10^{-1} to 1.4×10^{6} MPa$\sqrt{m}s^{-1}$ also has only a small effect on initiation fracture toughness.

In contrast, dynamic crack propagation toughness is strongly affected by α_p content. The 40% α_p microstructure has the highest propagation toughness ($K_{ID} \approx 120$ MPa$\sqrt{m}$), the 12% α_p microstructure has a somewhat lower toughness ($K_{ID} \approx$ 100 MPa$\sqrt{m}$), and the 0% α_p microstructure has significantly lower toughness ($K_{ID} \approx 65$ MPa$\sqrt{m}$). The dynamic propagation toughness for the α_p-containing microstructures is up to 70% higher than the dynamic initiation toughness. The increases in propagation toughness above the dynamic initiation toughness are due to a resistance curve effect associated with the formation of small shear lips during crack extension. The present results suggest that the tendency to form shear lips is a sensitive function of the microstructural condition. In the range of crack velocities investigated (50 to 450 m/s), dynamic propagation toughness was independent of crack velocity.

Scanning electron microscopy and fractography using fracture reconstruction applying surface topography analysis (FRASTA) showed that the proportion of intergranular failure decreases with increasing α_p content, that localized deformation within

grains or at grain boundaries is a dominant mechanism in microdamage initiation, and that microcracking ahead of the main crack front and often normal to the main crack plane plays an important role in the crack extension mechanism. High loading rates enhance the tendency for slip localization, leading to the formation of long tubular cavities, which markedly change the fracture surface morphology of all investigated microstructures. Crack tip opening displacement values obtained with FRASTA confirm the initiation toughness results.

A proposed microstructural damage model is outlined, and recommendations for further studies are presented.

ACKNOWLEDGMENTS

The authors would like to thank Dr. T. W. Duerig of Raychem Corporation, Menlo Park, California, for his assistance in selecting and characterizing the microstructures and for many helpful discussions of the results.

Particular thanks also go to Dr. G. Lee and Mr. Ladner of the United States Geological Survey in Menlo Park for preparing topographical maps of some of the fracture surfaces analyzed with FRASTA.

The authors would also like to acknowledge the contribution of A. T. Werner, their former colleague who performed the metallurgical study and the heat treatments of the alloy. F. Lovell, J. A. Kempf, E. P. Farley, J. Lemonds, T. S. Lovelace, D. Gandrud, M. A. Merritt, W. B. Heckman, and H. Rudnicki also contributed to the project.

CONTENTS

LIST OF FIGURES

LIST OF TABLES

SECTION 1

INTRODUCTION

Developments in the field of materials science are making possible the design of materials with prescribed properties. In an increasing number of situations, materials can be tailored or engineered for specific applications, such as the design of lighter, more maneuverable, and more fuel-efficient aircraft. Thus, engineered materials are a significant element in the effort to maintain a superior Air Force. Engineered materials often combine several monolithic materials or several phases to obtain the overall desired properties. Understanding and modeling the influence of each component material or phase and its interaction on the properties of multiphase materials is an important step in optimizing the performance of advanced engineered materials.

In recent years, the influence of loading rate on the behavior of materials has also been recognized. Changing the rate at which materials are stressed may change not only their flow properties but also the micromechanisms leading to their fracture. Quantitative evaluation of the effect of loading rate on the material response is therefore essential for designing structures such as aircraft or missiles that are subjected to a wide range of in-service loading rates.

This report summarizes the results of a three-year research program to investigate how microstructure and loading rate influence the fracture behavior of a promising advanced titanium alloy, Ti-10V-2Fe-3Al. This alloy is heat-treatable to a variety of microstructures and hence well suited for fundamental microstructure/properties studies. Moreover, because of its attractive strength-to-weight ratio, its good fracture properties, and its good formability, Ti-10V-2Fe-3Al is finding increasing use in aircraft structural components. The results obtained on this alloy are expected to be representative of an entire class of two-phase materials, so that the microdeformation and microdamage models developed will be more generally applicable.

In Section 2, we review the objectives and highlight the accomplishments of the program. The results are summarized in Section 3, and Section 4 outlines how the results of the present investigation could be incorporated into a model to simulate the behavior of the Ti-10V-2Fe-3Al microstructures. Finally, Section 5 lists the project personnel and describes special activities during the program. A list of publications and presentations resulting from this program and previous related programs (e.g., that sponsored under Contract No. AFOSR/F49620-81-K-0007) is also presented in Section 5.

SECTION 2

RESEARCH OBJECTIVES AND ACCOMPLISHMENTS

The objectives of this research were to establish how microstructural condition and loading rate influence the fracture behavior in an advanced titanium alloy, Ti-10V-2Fe-3Al, and to relate the macroscopic fracture toughness results to microscopic deformation and microdamage processes with a view toward developing microstructurally based fracture models.

To accomplish these objectives, we produced three Ti-10V-2Fe-3Al microstructures of comparable strength and grain size but with different primary alpha phase (α_p) contents, obtained by solution-treating the alloy at three temperatures. We then established the variation of the initiation toughness (K_{Id}) with loading rate and the propagation toughness (K_{ID}) with crack speed for the three Ti-10V-2Fe-3Al microstructures. We characterized the micromechanisms of failure for each microstructure and loading rate and determined some of the microstructural parameters controlling these mechanisms. We also obtained independent, microstructurally based toughness estimates by using local crack tip opening displacement measurements. On the basis of the experimental results, we outlined an approach to simulate computationally the microfracture behavior of the Ti-10V-2Fe-3Al microstructures.

The successful completion of this research program has resulted in the following significant accomplishments:

- We demonstrated that, for a given grain size distribution (50-300 μm), strength level (1280 ± 100 MPa), and loading rate, the solution treatment temperature and the resulting α_p content in the Ti-10V-2Fe-3Al microstructure has only a small influence on the initiation fracture toughness. Varying the solution treatment temperature between 760° and 820°C and the nominal α_p content from 40% to 0% decreases the toughness by less than 20%.

- Similarly, varying the loading rate from 2×10^{-1} to 1.4×10^{6} $MPa\sqrt{m}s^{-1}$ increases the initiation fracture toughness no more than 20% for a given Ti-10V-2Fe-3Al microstructure. These findings are confirmed by local crack tip opening displacement measurements obtained from the reconstructed fracture process by using FRASTA.

- In contrast, we established that the dynamic propagation toughness in the crack velocity range 50 to 450 m/s is independent of crack velocity but strongly affected by the α_p content. For a microstructure containing 40% α_p, the dynamic propagation toughness increases by over 50% above the dynamic initiation toughness, whereas for a microstructure with no α_p, the dynamic propagation toughness remains equal to the dynamic initiation toughness.

- The increase in dynamic propagation toughness above the dynamic initiation toughness observed in the α_p-containing microstructures can be attributed to a resistance curve effect associated with the formation of small shear lips during crack extension. The formation of the shear lips itself is a direct microstructural effect.

- From a fractographic point of view, the proportion of intergranular fracture increases with decreasing α_p content. Localized deformation within grains or at grain boundaries is a dominant mechanism in the initiation of microdamage. Microcracking ahead of the main crack front and often normal to the main crack plane plays an important role in the crack extension mechanism.

- High loading rates enhance the tendency for slip localization and markedly change the fracture surface morphology of all investigated microstructures.

SECTION 3

WORK PERFORMED AND RESULTS

MICROSTRUCTURES

The material studied in the present investigation was purchased from Timet Corporation in the original form of a 200-kg, 0.2-m-diameter billet. The chemical composition of the billet is reported in Table 1. The billet was first α–β forged to 50-mm-thick slabs and β-annealed at 843°C. The slabs were then β–rolled to 30 mm thick and α–β finish-rolled to 25 mm thick (Table 2). Figure 1 shows a three-orientation low magnification view of the as-received microstructure, which reveals a banding due to rolling. We established that the alloy had a β-transus of 810-815°C.

From the many possible microstructures that can be produced in the Ti-10V-2Fe-3Al alloy system, we chose to investigate microstructures with approximately the same strength level (1280 ± 100 MPa) but different α_p phase contents. To achieve the desired microstructures, we solution-treated at three temperatures to vary the α_p content and then varied the aging time and temperature to achieve approximately the same strength level.

The heat treatment for each microstructure is listed in Table 2. The corresponding microstructures are illustrated in Figure 2. The 820°C, or β-solution, treatment resulted in a microstructure without α_p (0% α_p). The 790°C and 760°C solution treatments resulted in microstructures with approximately 12% and 40% α_p content, respectively. We determined the α_p content by the point count grid method on small trial coupons used in a preliminary investigation to evaluate the solution treatment response of the as-received material. Subsequent metallography on heat-treated fracture specimens revealed some variability in the α_p from specimen to specimen for a given solution treatment. We also observed some inhomogeneity in the α_p content within a given specimen. Therefore, some fracture specimens solution-treated at 790°C may actually have a somewhat higher α_p content, and some fracture specimens solution-treated at 760°C may have a somewhat lower α_p content. Thus, the values of 40% and 12% α_p content are nominal values.

The 0% α_p microstructure had recrystallized equiaxed grains of 50-300 µm. A continuous α layer precipitated at the grain boundaries during aging. The α_p-containing microstructures had a more elongated grain structure resulting from the thermomechanical

TABLE 1
INGOT CHEMISTRY FOR Ti-10V-2Fe-3Al

	Fe	O_2	V	Mo	B	C	H	Sn	Cu	N	Al	Zr	Mn	Si
Top	1.850	.096	9.670	.031	.001	.014	1 ppm	.010	.001	.007	3.020	.001	.001	.034
Bot	2.040	.098	9.920	.031	.001	.021		.010	.002	.009	3.030	.001	.007	.044
Avg	1.945	.097	9.795	.031	.001	.017		.010	.001	.008	3.025	.001	.004	.039

TABLE 2
HEAT TREATMENT CONDITIONS FOR THREE MICROSTRUCTURES

Heat Treatment Steps \ % α_p	0%	12%	40%
Thermomechanical Treatment	α-β forged to 50-mm-thick slab, β annealed at 843° C, β rolled to 30-mm-thick plates, α-β finish-rolled to 25-mm-thick plates		
Solution Treatment	820° C for 1 h water quenched	790° C for 1h water quenched	760° C for 1 h water quenched
Aging Treatment	560° C for 1 h salt bath	535° C for 2.5 h salt bath	500° C for 8 h salt bath

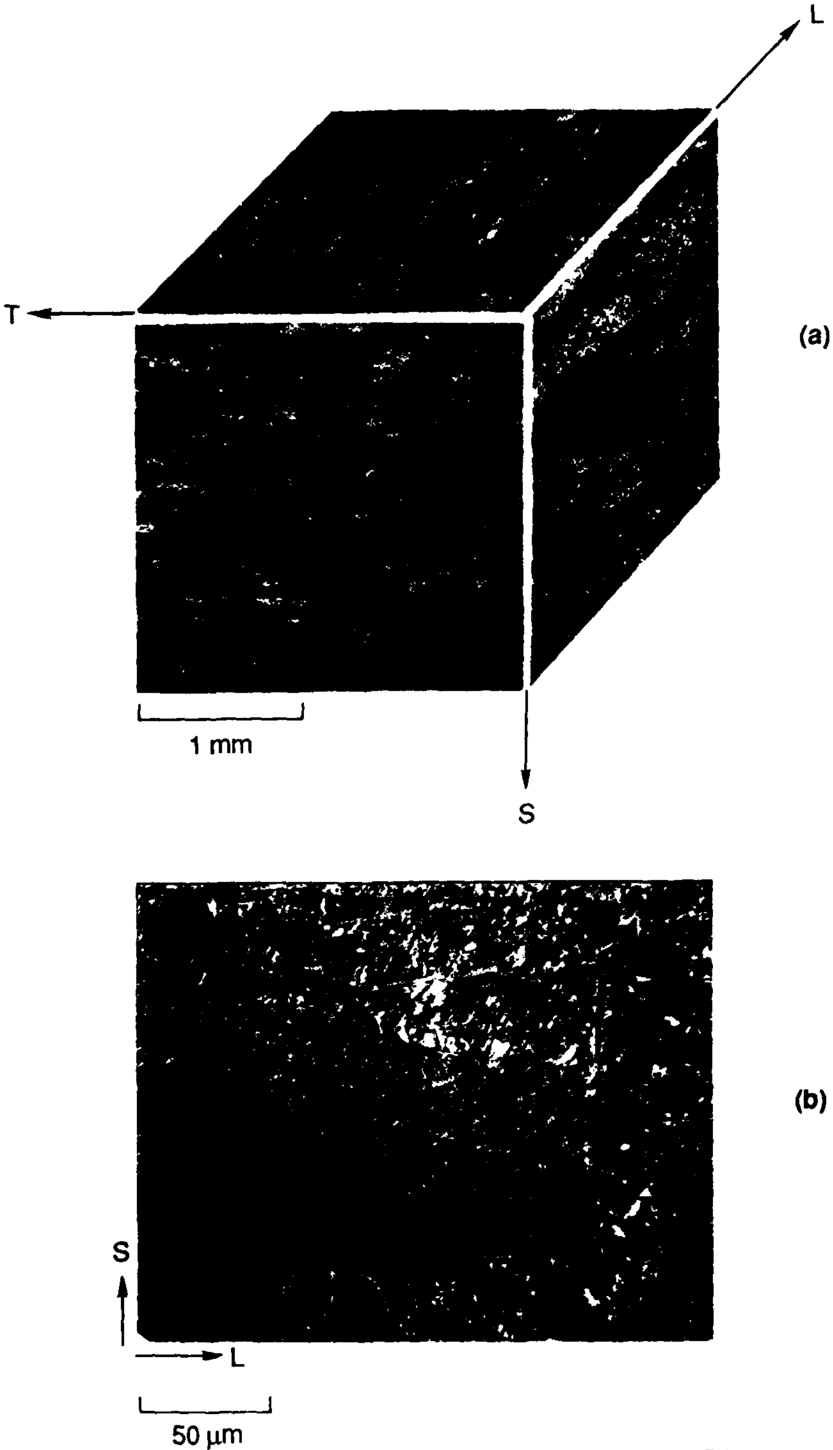

RP-1750-120

Figure 1. As-received microstructure of Ti-10V-2Fe-3Al;
(a) Three-orientation view,
(b) Detail of microstructure.

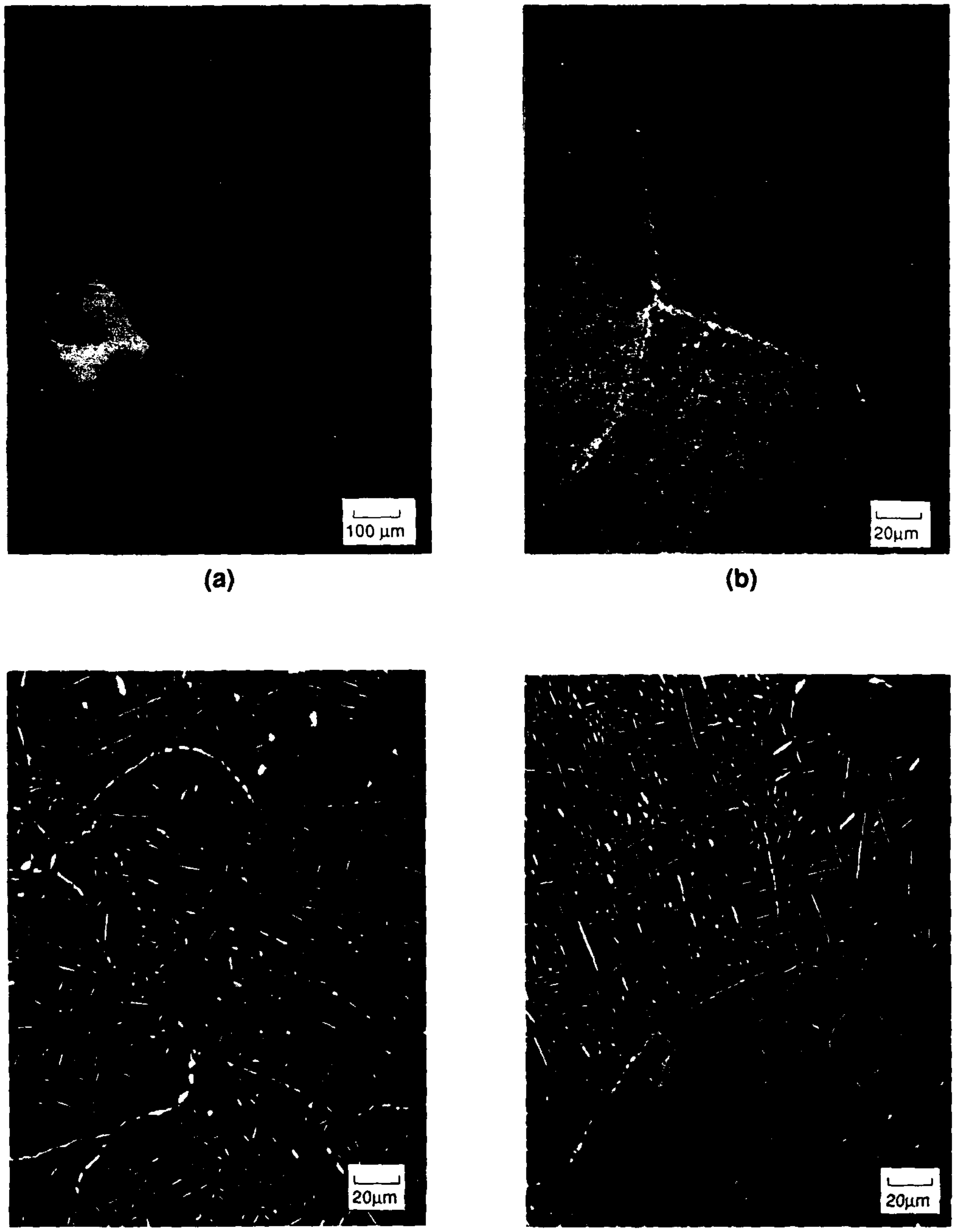

(c) (d)

RP-1750-121

Figure 2. Three investigated microstructures.
(a) and (b) 820° C ST, 0% α_p; (c) 790° C ST, 12% α_p (d) 760° C ST, 40% α_p.

treatment. The grain aspect ratio was roughly 1:2 to 1:4, and the grain size also varied between approximately 50 and 300 μm. We observed a variety of morphologies for the α_p phase, ranging from fine globular particles to elongated platelets. Some regions contained large globular α_p particles, while others had an agglomeration of thick platelets adjacent to a depleted region. The α_p-containing microstructures also had continuous and discontinuous grain boundary and sub-grain boundary α_p films. The tensile properties for the three microstructures are listed in Table 3. These properties were measured in duplicate with tensile bars heat-treated at the same time as the fracture specimens. The 0% and 40% α_p microstructures had almost identical stress-strain curves, whereas the 12% α_p microstructure had a strength 12% higher than that of the other two microstructures.

INITIATION FRACTURE TOUGHNESS MEASUREMENTS

Fracture initiation tests on the three microstructures selected for this program were performed at loading rates spanning a range from 2×10^{-1} MPa$\sqrt{m}$s^{-1} (static tests) to 2×10^{6} MPa$\sqrt{m}$s^{-1} (dynamic tests). We performed and analyzed the static tests according to ASTM Standard E399.[1] The tests used three-point-bend specimens.

The dynamic initiation toughnesses were obtained using the so-called one-point-bend (1PB) impact test, proposed and developed by Kanninen et al.[2] and Kalthoff et al.[3] and further developed at SRI under a previous AFOSR program.[4-6] In the 1PB impact test, a single-edge-cracked specimen is impacted by a moving hammer as in a conventional three-point-bend impact test, except that the specimen supports are omitted. The crack is loaded in bending solely by the inertia of the unsupported ends of the specimen. The resulting stress intensity history is a smoothly varying function of time and can conveniently be measured with a strain gage mounted near the original crack tip.

Figure 3 summarizes the results of the static and dynamic fracture initiation tests. Although the data are statistically sparse and there is considerable scatter (particularly for the 40% α_p microstructure), clear trends can be deduced from the initiation results.

At a given loading rate, decreases in α_p content from 40% to 0% are accompanied by decreases in initiation toughness of no more than 20% (63 to 56 MPa$\sqrt{m}$ and 75 to 62 MPa$\sqrt{m}$ for static and dynamic loading, respectively). The percent decrease seems to be slightly greater at high loading rates than at low loading rates. Changes in the loading rate from 2×10^{-1} MPa$\sqrt{m}$s^{-1} to 1.4×10^{6} MPa$\sqrt{m}$s^{-1} induce increases in the toughness of no more than 20%. The percent increase is largest for the 40% α_p microstructure.

TABLE 3
TENSILE PROPERTIES FOR THREE MICROSTRUCTURES

Property \ $\% \alpha_p$	0%	12%	40%
Yield Srength	1119 MPa	1257 MPa	1123 MPa
Ultimate Strength	1186 MPa	1327 MPa	1190 MPa
% Elongation	7.6	6.8	10.2

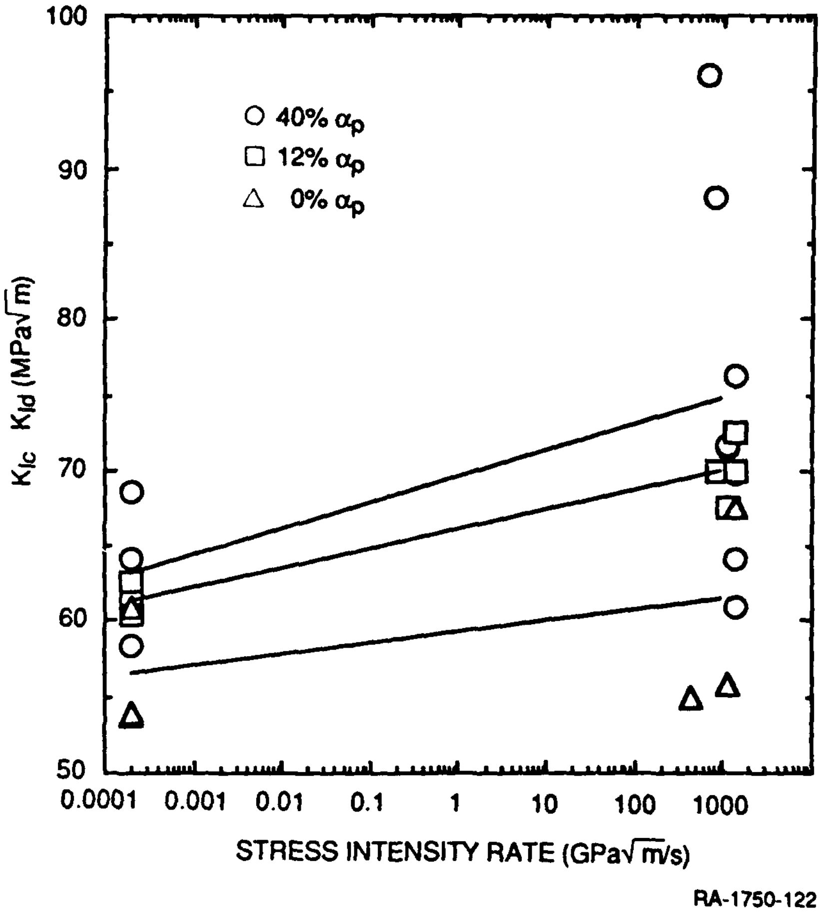

Figure 3. Summary of initiation toughness results.

Fractographic measurements of the crack tip opening displacement for selected specimens (reported below) confirm the relatively low sensitivity of the initiation toughness to α_p content and loading rate.

DYNAMIC PROPAGATION FRACTURE TOUGHNESS MEASUREMENTS

We again used the 1PB testing method to determine the dynamic propagation toughness. The experimental arrangement is shown in Figure 4. We added ballast plates to the specimen to augment its inertia and hence to achieve higher stress intensity amplitudes. During the crack propagation experiments we measured the impact velocity, the impact force (with strain gages mounted on the hammer), and the crack propagation history (by taking high-speed photographs of the ligament region of the specimen). We also measured strains normal to the crack plane at the initial crack or notch tip and at three locations spaced 10 mm apart along the crack path. These strain records provided independent verification of the crack propagation histories and coarse estimates of the stress intensity factor during crack propagation.

We controlled the loading rate and the crack velocity by adjusting the starting notch root radius and the impact velocity, (V_{imp}). Varying the root radius enabled us to control the amount of energy stored at crack initiation or, equivalently, the initiation stress intensity (K_{IQ}), and hence the crack velocity independently of the loading rate. In our experiments, crack velocities ranged from 50 to 450 m/s. Figure 5 shows a set of crack propagation histories produced in specimens of the 40% α_p microstructure by varying K_{IQ} and V_{imp}.

To obtain accurate values of the stress intensity factor at the tip of the extending crack, we applied a combined experimental-computational approach. We used the impact force, the time of crack initiation, and the crack extension history measured during 1PB experiments as inputs for dynamic finite element simulations of the experiments. In the simulations, we calculated the stress intensity history at the propagating crack tip by using a path independent domain integral[7].

In contrast to the results of the crack initiation experiments, we established that the dynamic propagation toughness K_{ID} was strongly affected by changes in α_p content. We found that, within the range of crack velocities investigated ($50 < \dot{a} < 450$ m/s), K_{ID} did not vary significantly with crack propagation velocity but did vary significantly with crack extension in the α_p-containing microstructures. This latter result is illustrated in Figure 6, which plots the dynamic propagation toughness K_{ID} as a function of the crack extension Δa for specimens of the three microstructures with blunt notches tested under identical

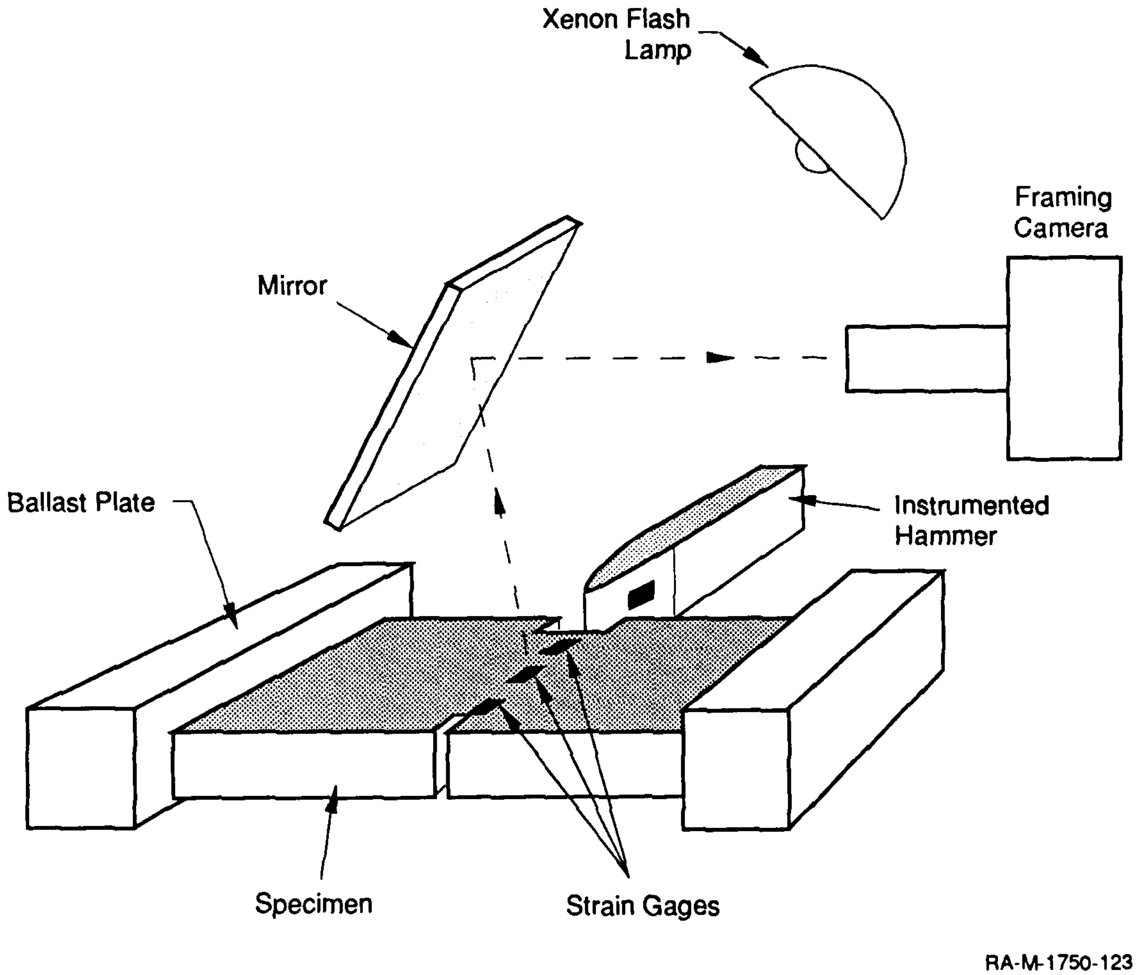

Figure 4. Experimental arrangement for the crack propagation experiments.

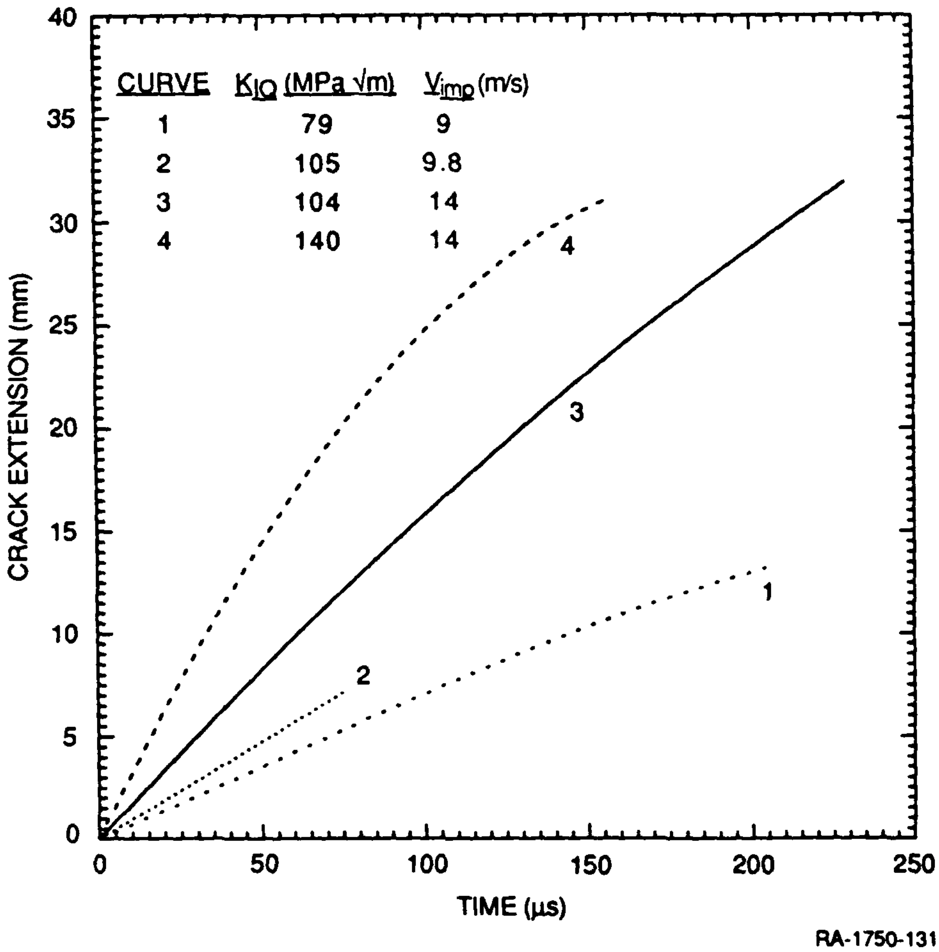

Figure 5. Crack propagation histories in 40% α_p microstructure.

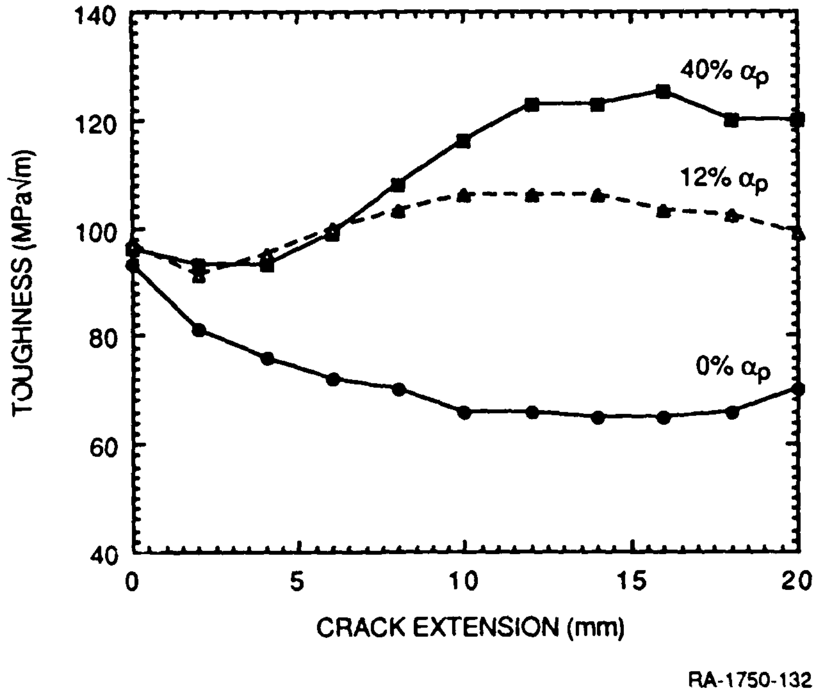

Figure 6. Dynamic propagation toughness versus crack extension distance for the 40% α_p, 12% α_p, and 0% α_p microstructures.

conditions, that is, a stress intensity value at initiation (K_{IQ}) of 95 MPa$\sqrt{m}$ and an impact velocity (V_{imp}) of 14 m/s. In the 0% α_p microstructure, K_{IQ} is higher than the material dynamic propagation toughness K_{ID}. Hence there is a drop in toughness during the first 5-10 mm of propagation, as the crack moves out of the initial notch plastic zone. After this transient phase, the dynamic propagation toughness remains essentially constant and equal to about 65 MPa$\sqrt{m}$. In contrast, in the two α_p-containing microstructures K_{ID} gradually rises above K_{IQ} after crack initiation to reach a steady-state value after approximately 5-10 mm of crack extension. Whereas the behavior in the transient phase of crack propagation depends on the value of K_{IQ} for a particular test, the steady-state value of K_{ID} is independent of the test conditions for all three microstructures.

The results of all the dynamic crack propagation experiments are summarized in Figure 7, which compares the steady-state dynamic propagation toughness to the dynamic initiation toughness for the three microstructures. The 40% α_p microstructure has the highest propagation toughness ($K_{ID} \approx 120$ MPa$\sqrt{m}$), the 12% α_p microstructure has a somewhat lower toughness ($K_{ID} \approx 100$ MPa$\sqrt{m}$), and the 0% α_p microstructure as significantly lower toughness ($K_{ID} \approx 65$ MPa$\sqrt{m}$). Figure 7 demonstrates that the steady state value of K_{ID} is significantly higher than the dynamic initiation toughness (K_{Id}) for the α_p-containing microstructures, whereas K_{ID} is approximately the same as K_{Id} for the 0% α_p microstructure.

The effect of the difference in propagation toughness on dynamic crack extension is illustrated in Figure 8, which shows the fracture surfaces of fatigue precracked specimens with 40%, 12%, and 0% α_p impacted at 14 m/s. In the 40% and 12% α_p specimens, cracks were dynamically initiated and arrested, then marked by fatiguing and extended to completion statically. The crack traversed the 0% α_p specimen without arresting. The arrest lengths give an indication of K_{ID}, with the shortest arrest length occurring in the toughest material, which is the 40% α_p microstructure. The photographs also show that the shear lip height varies inversely with the arrest length, being largest for the 40% α_p microstructure and smallest for the 0% α_p microstructure.

On the basis of the observation that the shear lip size increases with α_p content and the dynamic propagation toughness increases with the amount of crack extension (resistance curve effect) in the α_p-containing microstructures, we conclude that the shear lips play a dominant role in controlling the dynamic propagation toughness. The small differences in initiation toughness and yield stress in the three microstructures are sufficient to promote the formation of plastic zones and hence shear lips of different sizes depending

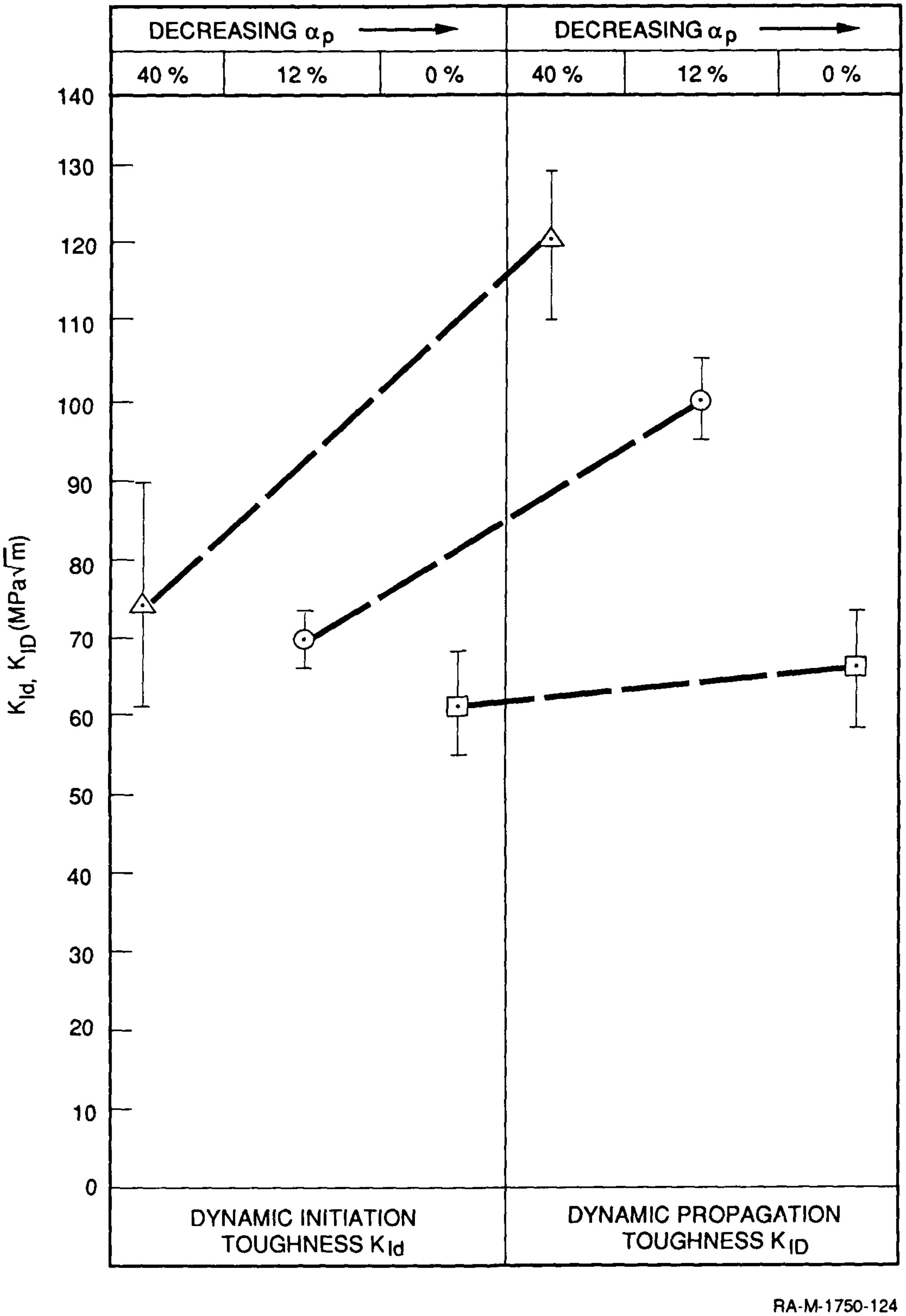

Figure 7. Comparison of dynamic initiation and propagation toughness.

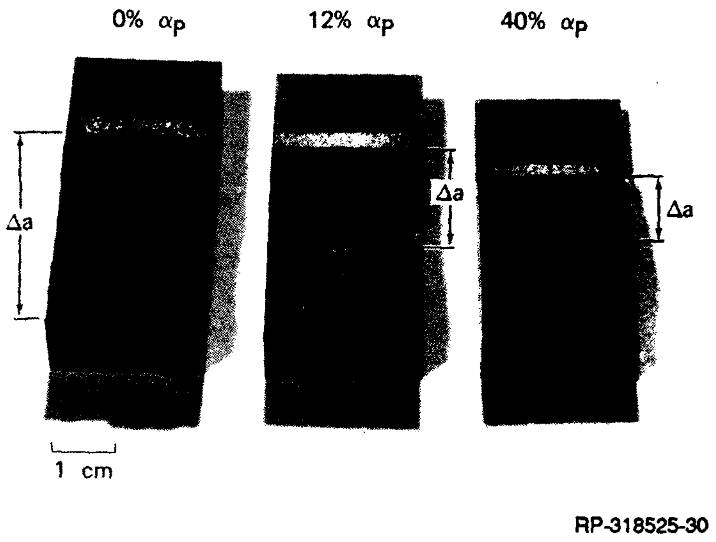

Figure 8. Fracture surfaces of the three microstructures tested under identical dynamic conditions.

on the α_p content. As the crack extends, shear lips act as trailing tensile ligaments; they force the crack front to gradually bow, and they effectively raise the apparent fracture toughness. In turn, the higher apparent toughness promotes larger shear lips. This coupled mechanism is most pronounced in the 40% α_p microstructure, which has the largest estimated initial plastic zone, and least pronounced in the 0% α_p microstructure, which has the smallest estimated initial plastic zone. This postulated mechanism implies that shear lips are simultaneously the cause and the evidence of the increase in propagation toughness with crack extension. The influence of shear lips on propagation toughness is in itself a structural rather then a microstructural effect. However, our results suggest that the tendency to form shear lips is a sensitive function of the microstructural condition. The dynamic resistance curve concept linked to the formation of shear lips was invoked earlier to explain similar dynamic fracture observations in high-strength steel[4].

FRACTOGRAPHIC RESULTS

We performed scanning electron microscope (SEM) observations of tensile and fracture specimens. Selected specimens were then analyzed with the FRASTA (fracture reconstruction applying surface topography analysis) method.[8] FRASTA is an advanced posttest fractographic method that uses a computer technique to compare quantitative three-dimensional topographs of conjugate fracture surfaces (matching fracture surfaces from each half of a broken specimen) and to reconstruct the details of the fracture process. FRASTA also provides a direct measurement of the crack tip opening displacement (CTOD). These fractographic observations were complemented by observations of polished and etched cross sections normal to the crack plane to evaluate collateral damage and to establish the initiation site for microcracks and microvoids.

The fracture surface appearance near the fatigue crack tip region of statically and dynamically loaded specimens with 40%, 12% and 0% α_p is compared in Figure 9. We identified two size scales for the fracture surface features. The larger scale is on the order of many tens of micrometers to several several hundred micrometers. Fractographic features on this scale include features that are all related directly or indirectly to the grain size (such as grain facets, grain fragments, microcracks, and large stretch or slip regions), which suggests that the grain size may play an important role in controlling the fracture behavior. The smaller scale is on the order of many micrometers. Fractographic features on this scale consist predominantly of microvoids and often cover the surface of the larger scale features. The morphology, size, and density of the microvoids depend not only on

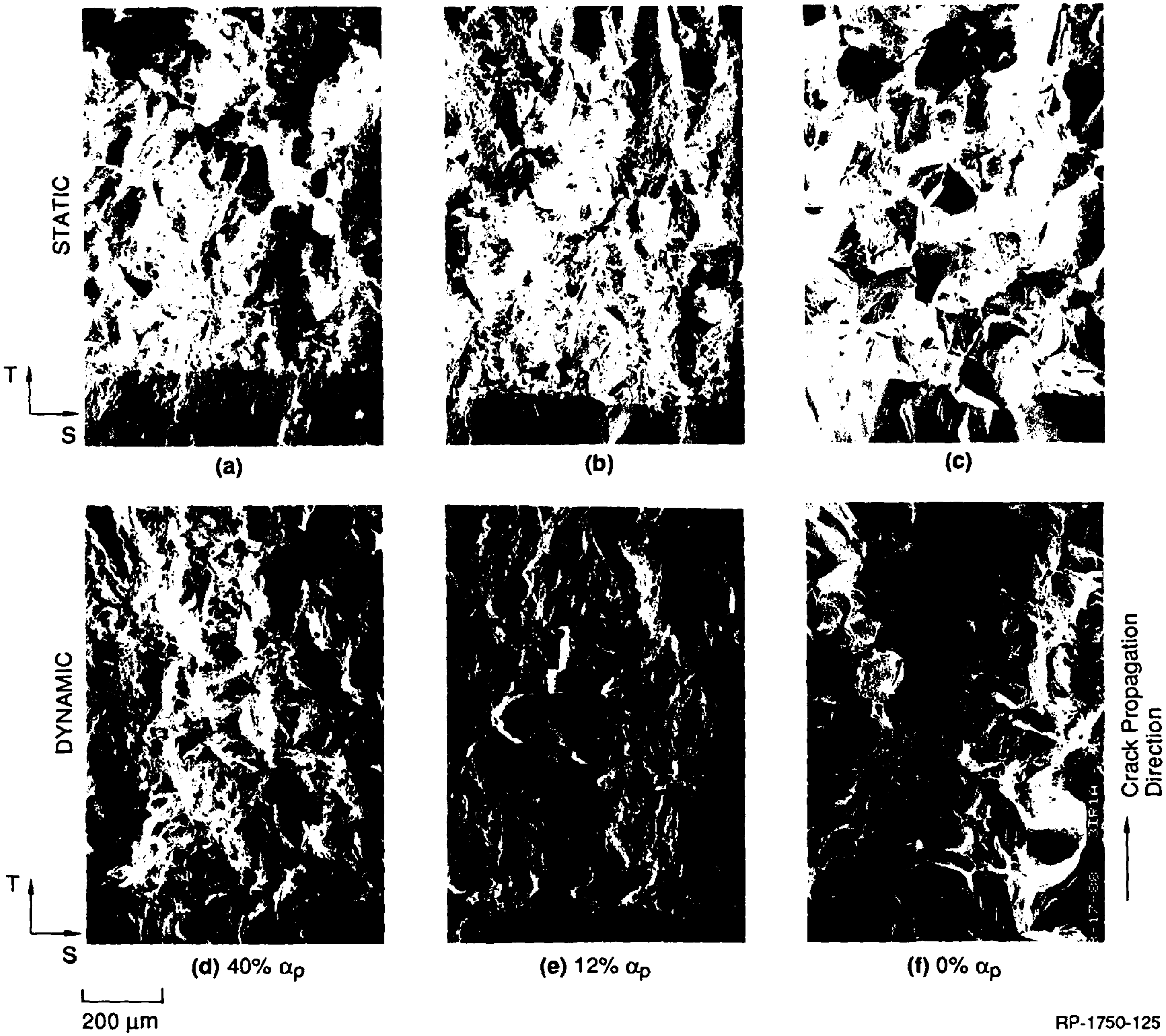

Figure 9. Fracture surfaces of statically and dynamically loaded Ti-10V-2Fe-3Al specimens.

(a) and (d) 760° C ST, 40% α_p; (b) and (e) 790° C ST, 12% α_p (c) and (f) 820° C ST, 0% α_p.

the microstructure and the loading rate but also on the local deformation history (ratio of tensile to shear deformation).

In all three microstructures and for all strain rates, we observed some transgranular fracture and some intergranular fracture. The proportion of transgranular fracture decreased with decreasing α_p content: the 40 % α_p microstructure failed predominantly by transgranular fracture, whereas the 0% α_p microstructure failed predominantly by intergranular fracture. For all microstructures and strain rates, we also found much evidence of localized slip across grains and in the grain boundary α phase, which indicates that localized slip plays a key role in the nucleation and growth of microfracture. In the α_p-containing microstructures, microvoids nucleated preferentially at α_p platelets, and cracks tended to follow grain or subgrain boundary α_p films or rows of α_p particles. For the microstructure with no α_p, voids also nucleated at grain boundaries, and microcracks to a large extent followed the grain boundary α film. These fractographic observations are consistent with previously published results on the microdeformation and fracture mechanisms of Ti-10V-2Fe-3Al microstructures.[9,10]

In addition, our investigation provides several new significant results. First, we found many transverse microcracks normal to the main crack plane. These predominantly intergranular transverse microcracks are observed in all microstructures and can be many tens of micrometers in width and depth and present a significant opening in the main crack plane. Therefore, the process of forming transverse microcracks involves significant deformations parallel to the main crack plane, which will have a bearing on the interpretation of FRASTA results below. Figure 10 shows two examples of transverse microcracks (indicated by arrows) in the 0% α_p microstructure and Figure 11 shows an example for the 40% α_p microstructure.

Second, we found that localized slip is greatly enhanced by higher loading rates. This rate sensitivity appears strongest in the 12% α_p microstructure and lowest in the 0% α_p microstructure. Figure 11 shows an example of large slip deformation observed near a transverse crack in a dynamically loaded specimen of the 40% α_p microstructure. The large microcrack formed possibly at a grain or subgrain boundary. The visible tip of the microcrack has been blunted by slip of four independent blocks of material (numbered 1 through 4 in Figure 11) on at least two slip planes (indicated by arrows in Figure 11). Note the smooth appearance of the slip surfaces. We also made similar observations of localized slip in the other two microstructures. Rate-enhanced slip deformations can lead to the formation of long tubular cavities, as illustrated in Figure 12. The figure shows a series

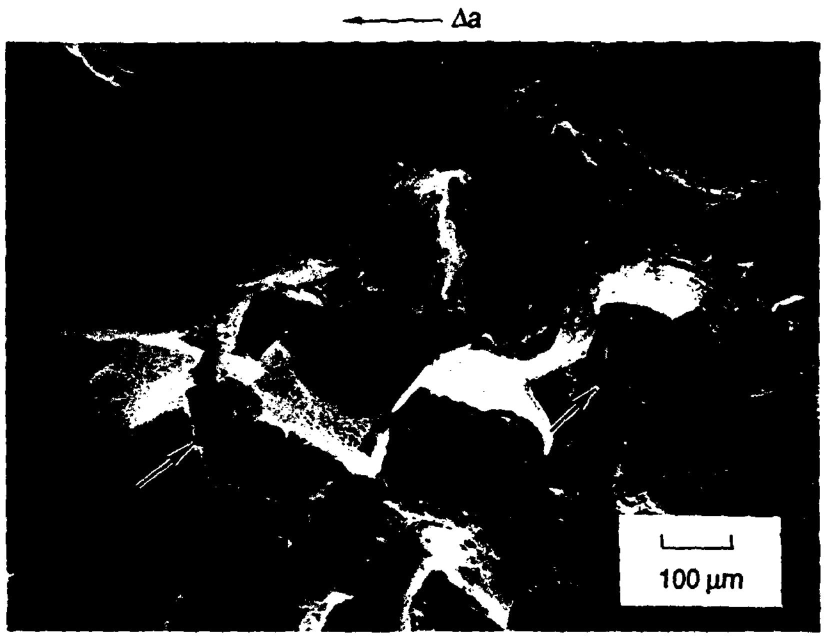

RP-1750-126

Figure 10. Transverse microcracks (indicated by arrows) in the fracture surface of a dynamically loaded specimen of 820° C ST, 0% α_p microstructure (crack propagation region).

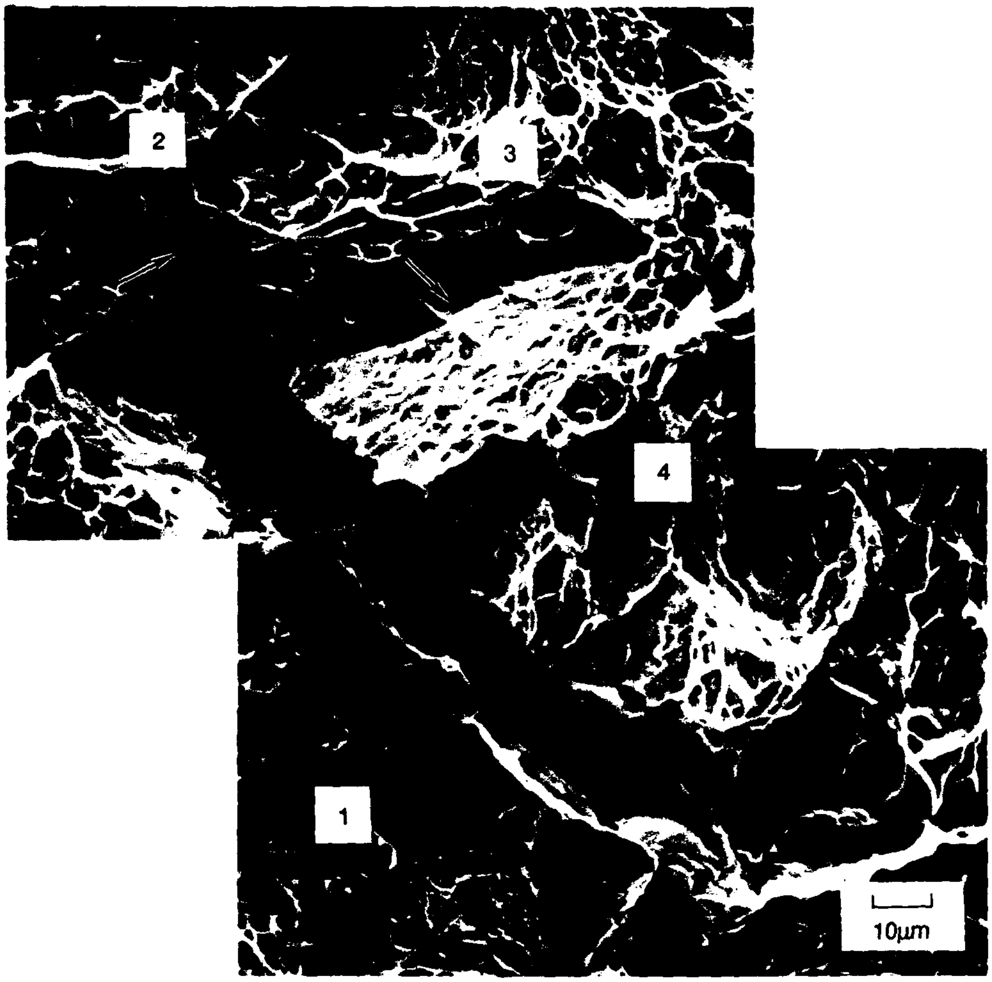

RP-1750-127

Figure 11. Transverse microcrack and localized slip in the fracture surface of a dynamically loaded specimen of 760° C ST, 40% α_p microstructure (crack propagation region). Slip planes indicated by arrows.

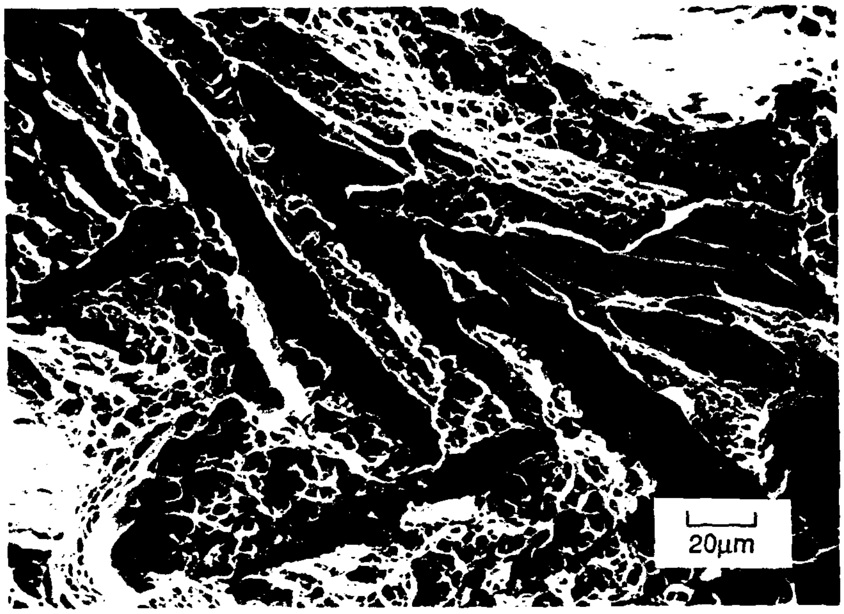

RP-1750-128

Figure 12. Localized deformation forming a herringbone pattern in the fracture surface of a dynamically loaded spcimen of 820° C ST, 0% α_p microstructure (detail of Figure 7f).

of long, smooth channels forming a herringbone pattern on the fracture surface of a dynamically loaded specimen of the 0% α_p microstructure. We observed a similar herringbone pattern on the other fracture surface of the specimen, and matching of the two patterns demonstrates that they represent two halves of hollow tubes. We think these tubes were produced by slip steps formed by localized slip on a series of neighboring planes and interaction with a soft grain boundary. The material between the tubes then failed by void nucleation and growth. Numerous isolated smooth channels similar to those shown in Figure 12 were also found in the α_p-containing microstructures.

Third, FRASTA and detailed fractography demonstrate that the fracture process is discontinuous along the crack front, as illustrated in Figure 13 for a dynamically loaded specimen of the 0% α_p microstructure (see the area analyzed in Figure 7f). Figure 13 shows a series of so-called Fractured Area Projection Plots (FAPPs) as a function of topographic displacement obtained with FRASTA. FAPPs are equivalent to X-radiographs, taken normal to the nominal fracture plane, to observe microcrack formation in the crack plane region (white in Figure 13). The FAPPs provide information on the locations of the microcrack initiation sites and the projected areas of the microcracks or cracks.

In Figure 13, the initial fatigue crack front is at the bottom of the plot and the crack *moves from bottom to top*. Figure 11a shows the FAPP corresponding to a state of crack opening just before the initiation of microcrack advance. Many microcracks form ahead of the main crack. By superposing the FAPP on the SEM photographs, we can establish the fractographic features with which the microcracks are associated. We found that microcracking ahead of the main crack front observed in the FAPPs often corresponds in SEM photographs to transverse microcracks along grain boundaries or across grains*. Therefore, FRASTA reveals that some material regions fracture early in the crack opening process, leaving behind uncracked ligaments that fail at a later stage of deformation.

We believe that the observed microcracking may play an essential role in controlling the growth of the main crack front. Depending on their orientation, microcracks can locally

---

* Because these microcracks form so far in advance of the fatigue crack front, the question arises whether they are a real feature of the fracture process or an artifact of the FRASTA reconstruction. A detailed fractographic study demonstrates that the region of microcracking indeed fails before the arrival of the main crack front. However, because FRASTA only considers the sequence of deformation normal to the main crack plane and does not account for the in-plane deformation, the sequence in which the microcracks (formed by in-plane displacements) appear with respect to the extending main crack is not always predicted accurately. Thus, the microcracks shown in the FAPPs are real, but they may in some cases be formed in the fracture specimen at a larger crack opening than indicated by the FAPPs.

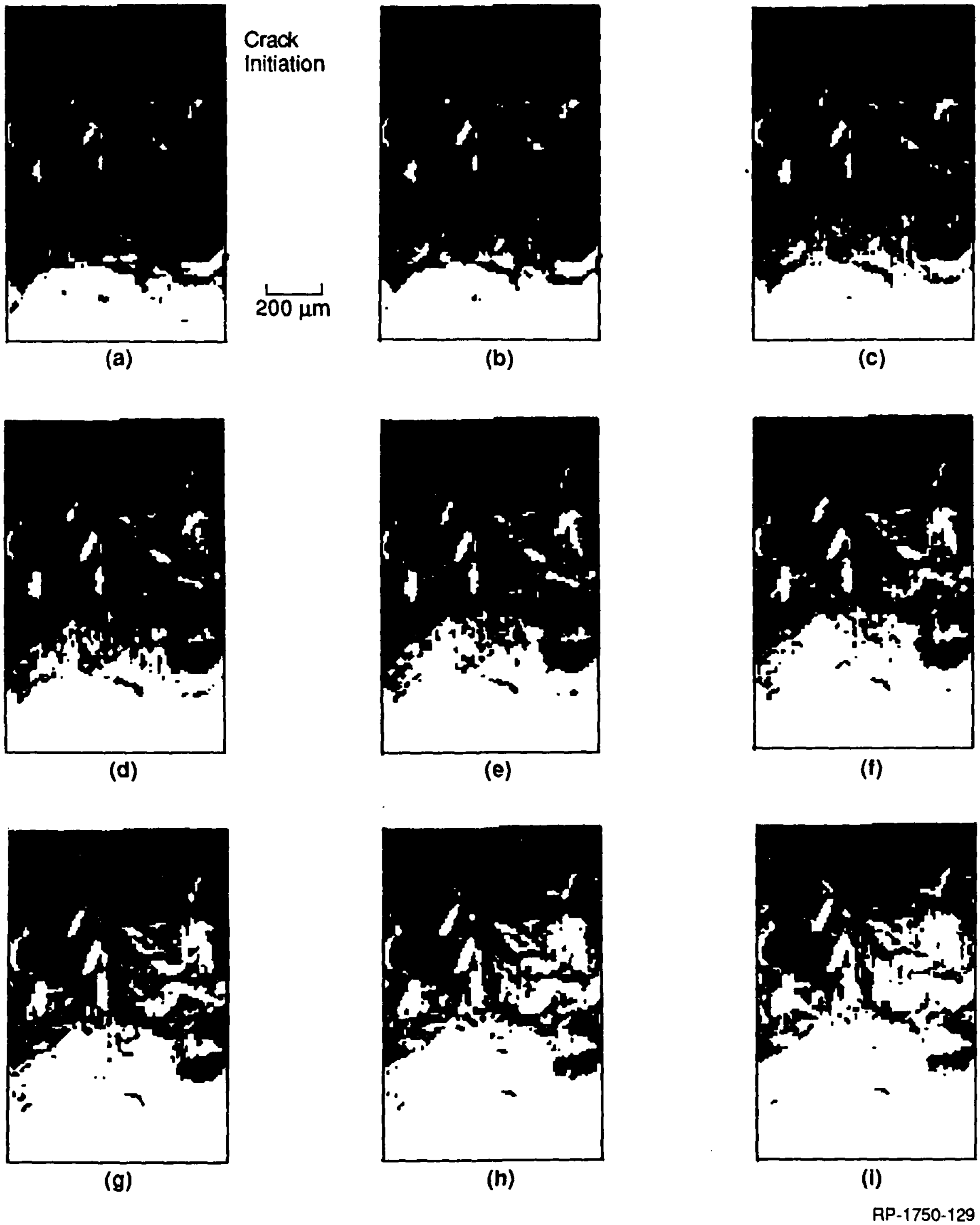

Figure 13. Fractured area projection plots as a function of crack opening for a dynamically loaded specimen of 820° C ST, 0% α_p microstructure. Area corresponds to area in Figure 7f. (Fracture surfaces separation increment between each plot, 6.9 μm.)

blunt the advancing main crack and increase the local deformation required for further crack extension. Moreover, microcracks can relax the deformation constraint on the adjacent material, a change that can transfer stresses from one material region to another and induce new, more favorable deformation modes. As a result, the material in the unbroken region can undergo larger strains before fracture and may fail by a different mechanism than when it is fully constrained.

With FRASTA, we also measured the CTOD at the tip of the initial fatigue crack to obtain an independent, microstructurally base measure of toughness. The results for the four specimens we analyzed (one statically loaded and one dynamically loaded specimen each for the 40% α_p and the 0% α_p microstructures) are shown in Table 4. The CTOD determined from FRASTA can be related to the J-integral or stress intensity factor to independently assess the fracture toughness as a function of microstructural or loading conditions. Here we used the following equation to relate crack opening displacement to toughness expressed in terms of the stress intensity factor:

$$K_{Ic}, K_{Id} = \sqrt{E\, \sigma_{flow}\, CTOD/(1-\nu^2)} \qquad (1)$$

where K_{Ic} and K_{Id} are the toughness of statically and dynamically loaded specimens, respectively; E is Young's modulus; ν is Poisson's ratio; and σ_{flow} is the average of the static yield stress and the ultimate stress. Table 4 also list the converted toughness values and compares them with the values measured in the fracture experiments for the specimens analyzed with FRASTA.

For a given loading rate, the CTOD values for the 40% α_p and the 0% α_p microstructures are similar and confirm the result of the fracture toughness test, which indicated only relatively small differences between the toughnesses of the various microstructures. The rate sensitivity of fracture initiation in the 40% α_p microstructure predicted by the CTOD measurements is consistent with that established with the stress intensity factor based-toughness measurement. For the 0% α_p microstructure, the CTOD measurements overpredict the rate sensitivity.

The toughness values obtained from the CTOD values and Equation (1) are within about 20% or better of the measured values and tend to underpredict the toughness, except for the dynamically loaded specimen of the 0% α_p microstructure, where the initiation toughness is overpredicted. The agreement between CTOD-derived and directly measured toughness confirms FRASTA's ability to determine fracture toughnesses from broken specimens.

TABLE 4
CRACK TIP OPENING DISPLACEMENT (CTOD), CTOD-DERIVED TOUGHNESS (K_I), AND MEASURED TOUGHNESS FOR SELECTED SPECIMENS OF Ti-10V-2 Fe-3Al ALLOY

	40%			0%		
	CTOD (μm)	Calculated K_I at Initiation* ($MPa\sqrt{m}$)	Measured K_I at initiation ($MPa\sqrt{m}$)	CTOD (μm)	Calculated K_I at initiation* ($MPa\sqrt{m}$)	Measured K_I at initiation ($MPa\sqrt{m}$)
Static	21	53	58	19	50	61
Dynamic	33	67	72	34	68	56

* Calculated using equation (1).

SECTION 4

OUTLINE OF A MICROSTRUCTURAL DAMAGE MODEL AND RECOMMENDATIONS FOR FURTHER STUDIES

The ultimate goal of detailed microstructure properties investigations is to develop models for predicting the microstructure characteristics required to obtain specific material properties. In this section, we outline a modeling approach to incorporate and rationalize the results of the present investigation, and we make recommendations for additional studies in support of the model development.

The present study points out the complexity of the often competing failure processes in the Ti-10V-2Fe-3Al microstructures. Whether intergranular or transgranular fracture occurs depends on many factors such as distribution of the grain boundary α, morphology and distribution of the α_p phase, and orientation of the grains with respect to the local stress and deformation field. The present study also points out some key features that should be included in a damage model for the Ti-10V-2Fe-3Al microstructures, namely, slip localization, the rate sensitivity of slip localization, and grain boundary failure in the soft α-phase film. Indeed, the observations of these three key features in all three microstructures may provide the explanation for the similarity in their fracture behavior, at least in what concerns crack initiation.

The similarity also suggests a possible approach for modeling the microfracture of some Ti-10V-2Fe-3Al microstructures. As sketched in Figure 14, the Ti-10V-2Fe-3Al microstructure is represented by a set of two-dimensional grains consisting of two materials, one forming the bulk of the grain, the other forming the grain boundary α phase. The strength and fracture properties of both materials can be varied independently to simulate the strength differential observed in the actual microstructure.

For modeling the grain boundary material, we suggest using a material with a constitutive behavior based on isotropic plasticity but including a damage model to simulate void nucleation and growth processes. A damage model in which the void growth rate depends on both the applied plastic strain and the ratio of mean to equivalent stress appears adequate. Such a model is available at SRI and has previously been used to simulate fracture of ductile steels.[11]

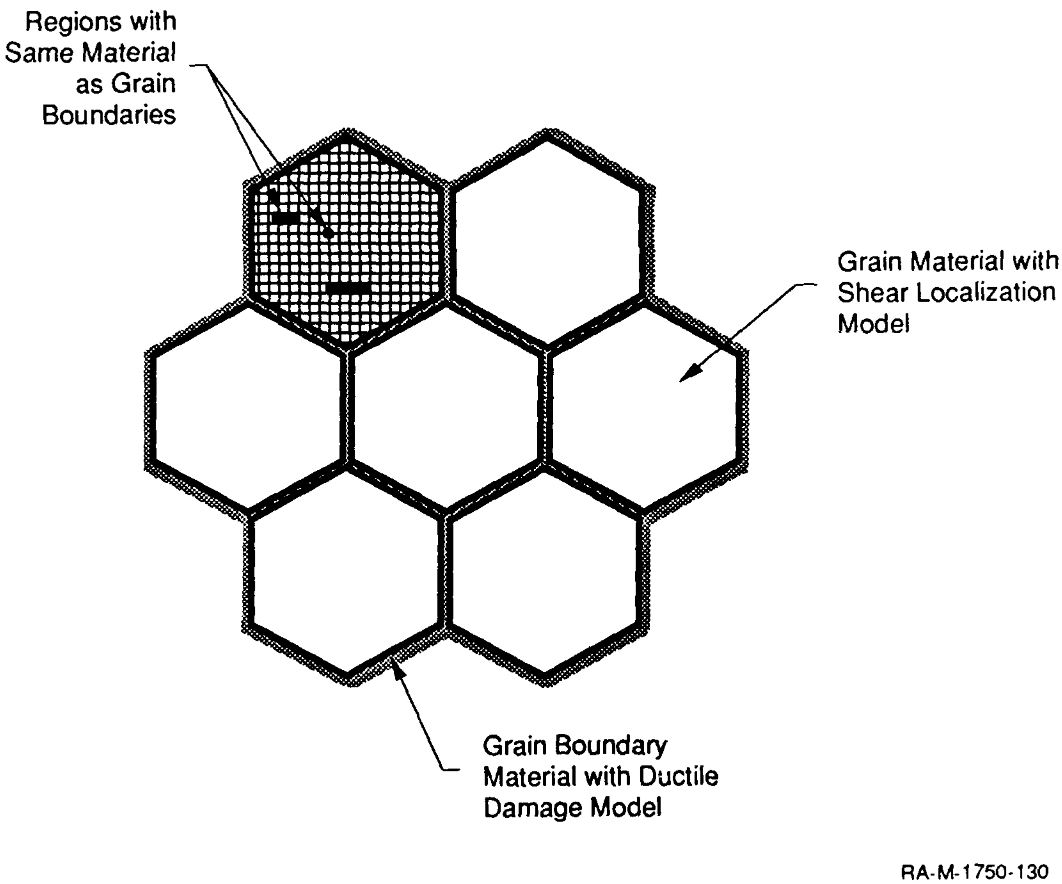

Figure 14. Suggested model for the investigated Ti-10V-2Fe-3Al micro-structures.

To account for slip localization within the grains, we envision using for the grain material a plasticity model in which plastic deformation is partitioned on a limited number of distinct planes. This approach allows anisotropic plastic deformation to develop and strain localization to occur in a natural way. Such a plasticity model has also been developed at SRI to model adiabatic shear bands (SHEAR4 model).[11] The model is strain rate sensitive and includes mechanisms to allow tensile fracture to develop on weakened shear planes. Variations in matrix strength due to different aging treatments can be introduced by varying the shear strength of individual planes in the SHEAR4 models. In a first approximation, this approach could also be used to simulate the effect of different distributions and morphologies of the α_p phase, that result from different thermomechanical treatments and solution treatments. Alternatively, a more detailed model could be introduced for the grains, in which individual α_p particles would also be represented. This representation could be accomplished by zoning up the grains more finely and assigning to some regions simulating the α_p particles the same material and damage model assigned to the grain boundaries.

The fractographic observations and the results of the fracture tests obtained in this study can be used for the development and calibration of the model. The model can then be used to evaluate the effect of microstructural changes on fracture properties in order to optimize the processing and heat-treatment for the alloy without performing an extensive testing program. The model could also be extended to other alloys having a similar morphology.

Clearly, although the basic material models and a significant body of experimental data are available to support the modeling effort, considerably more work will be required to be able to model in detail the results of this study and to predict the effect of microstructural modifications. To support the modeling effort, we recommend additional fractographic and metallographic observations to establish in more detail the mechanisms of slip localization, grain boundary fracture, and void nucleation at α_p particles and at α_s (secondary α) platelets. In particular, our study and other studies[10] suggest that the grain size may have a significant effect on the fracture behavior of Ti-10V-2Fe-3Al microstructures. We therefore recommend that additional static and dynamic fracture experiments be performed on microstructures with similar strength and α_p contents (within the limits imposed by the metallurgical behavior of the alloy) but with finer grains.

Independently of the microdamage modeling effort, the role of shear lips in controlling the propagation toughness should be further investigated. Available models for the influence of trailing ductile ligaments on the effective toughness of steels failing by cleavage should be applied to the shear lip problem to quantify the contribution of the shear lips to the measured dynamic propagation toughness. To support this modeling effort, we recommend performing static fracture experiments to determine the toughness resistance curve and to establish if the effect of shear lips is similar under static and dynamic loading conditions. Additional static and dynamic crack propagation experiments with side-grooved specimens (to suppress the formation of shear lips) will allow a quantitative assessement of the contribution of shear lips to the propagation toughness. Moreover, the dynamic stress-strain curve of the three microstructures should be measured to determine if differences in the dynamic flow behavior could be responsible for the difference in shear lip size observed in the dynamic crack propagation experiments.

SECTION 5

PERSONNEL, ACTIVITIES, PUBLICATIONS, AND PRESENTATIONS

PERSONNEL

The following professional personnel were associated with this research effort

Dr. J. H. Giovanola, Principal Investigator

Dr. D. A. Shockey, Principal Investigator

Dr. R. W. Klopp

Dr. J. W. Simons

Dr. T. Kobayashi

Mr. A. T. Werner

Dr. J. Lemonds

Dr. T. Duerig, consultant

ACTIVITIES

The work performed in this program was presented at the Seventh International Conference on Fracture (ICF7) held in Houston on March 20-24, 1989, and a paper was published in the Proceedings of the Conference. Two additional papers are in preparation: one covering the fractographic observations will be submitted to *Metallurgical Transactions*, and one covering the experimental and continuum mechanics aspects of the investigation will be submitted to *Engineering Fracture Mechanics*. In addition, some of the experimental results obtained in the previous program[4] were included in a Technical Note recently published in *Journal for Testing and Evaluation.*

The work performed in this and the previous program continue to attract the attention of the technical and scientific community. The Principal Investigators, Drs. Shockey and Giovanola have been invited to attend and make a presentation at the Oji International Seminar on Dynamic Fracture (Toyohashi,Japan, August 1-4, 1989) sponsored by the Japan Society for the Promotion of Science and the Fujihara Foundation of Science. Furthermore, Dr. Shockey gave the Invited Lecture on Recent Progress on Dynamic Fracture Testing and Treatment at Impact 87, International Conference on Impact Loading and Dynamic Behaviour of Materials (Bremen, FRG, May 18-22, 1987) and has organized a session on dynamic fracture at the joint ASME-JSME 1989 Pressure Vessel and Piping Conference (Hawaii, July 23-27,1989).

Extensive oral reviews of the program results were given to Dr. A. H. Rosenstein of the Air Force Office of Scientific Research (AFOSR) during his yearly visits to SRI. The results were also presented to the Fatigue and Fracture Branch of the David Taylor Naval Ship Research and Development Center, Annapolis, MD.

Dr. Giovanola has been invited on several occasions to lecture on dynamic fracture at the University of California at Berkeley.

From a more practical point of view, the experience and knowledge acquired during these AFOSR-sponsored research programs directly benefitted the Air Force when Dr. Giovanola acted as a consultant on dynamic crack propagation during the investigation of the TITAN 34D-9 mishap.

PUBLICATIONS

J. F. Kalthoff and D. A. Shockey, "Instability of Cracks Under Impulse Loads, " J. Appl. Phys. **48**, 984-993 (March 1977).

D. A. Shockey, J. F. Kalthoff, H. Homma, and D. C. Erlich, "Criterion for Crack Instability Under Short Pulse Loads," in *Advances in Fracture Research*, D. Francois et al., Eds. (Oxford and Pergamon Press, New York, 1980), pp. 415-423.

D. A. Shockey, J. F. Kalthoff, and D. C. Erlich, "Evaluation of Dynamic Crack Instability Criteria," Int. J. Fract. Mech. **22**, 217-229 (1983).

D. A. Shockey, J. F. Kalthoff, W. Klemm, and S. Winkler, "Simultaneous Measurements of Stress Intensity and Toughness for Fast Running Cracks in Steel," Exp. Mech. **23**, 140-145 (1983).

H. Homma, D. A. Shockey, and Y. Murayama, "Response of Cracks in Structural Materials to Short Pulse Loads," J. Mech. Phys. Solids **31**, 261-279 (1983).

D. A. Shockey, J. F. Kalthoff, H. Homma, and D. C. Erlich, "Response of Cracks to Short Pulse Loads," in *Proceedings of the Workshop on Dynamic Fracture*, a workshop held at the California Institute of Technology, Pasadena, CA, February 17-18, 1983, under sponsorship of the National Science Foundation and the Army Research Office, W. G. Knauss, Ed. (Caltech Press, 1983), pp. 57-71.

J. H. Giovanola, "Investigation and Application of the One-Point-Bend Impact Test," in *Fracture Mechanics: Seventeenth Volume*, ASTM STP 905, J. G. Underwood, R. Chait, C. W. Smith, D. P. Wilhelm, W. A. Andrews, and J. Newman, Eds. (American Society for Testing and Materials, Philadelphia, 1986), pp. 307-328.

J. H. Giovanola, "The One-Point-Bend Test," in *ASM Metals Handbook*, 9th Edition, Volume 8, *Mechanical Testing* (American Society for Metals, Metals Park, OH, 1985), pp. 271-275.

D. A. Shockey, "Short-Pulse-Duration Tests," in *ASM Metals Handbook*, 9th Edition, Volume 8, *Mechanical Testing* (American Society for Metals, Metals Park, OH 1985), pp. 282-284.

D. A. Shockey, J. F. Kalthoff, H. Homma, and D. C. Erlich, "Short Pulse Fracture Mechanics," in *Dynamic Fracture, The Albert S. Kobayashi Anniversary Volume of the International Journal of Fracture*, M. F. Kanninen and S. N. Atluri, Eds. (Pergamon Press, New York, 1986), pp. 311-319.

J. H. Giovanola, "Crack Initiation and Extension in Steel for Short Loading Times," in *Proceedings of DYMAT 85 Conference on Mechanical and Physical Behavior of Materials under Dynamic Loading*, Paris, September 2-5, 1985, (Les Editions de Physique, France, 1985), pp. C5-171 through C5-178.

D. A. Shockey, "Recent Progress in Dynamic Fracture Testing and Treatment" in *International Conference on Impact Loading and Dynamic Behavior of Materials*, C. Y. Chiem et al., Eds.), (DGM Informationsgeselschaft mbH, Oberursel, FRG, 1988), pp. 3-21.

J. H. Giovanola, T. Kobayashi, R. W. Klopp, T. Gaines, and R. Arwood, "A Note on Dynamic Displacement Measurements Using Hall Effect Sensors," Journal for Testing and Evaluation, **17**, 196-200 (1989).

J. H. Giovanola, R. W. Klopp, D. A. Shockey, and A. T. Werner, "Effect of Microstructure and Loading Rate on the Fracture Behavior of Titanium-10V-2Fe-3Al," in *Advances in Fracture Research*, Vol. 1, *Proceedings of the Seventh International Conference on Fracture*, Houston, March 20-24, 1989, K. Salama et al., Eds. (Pergamon Press, New York, 1989), pp. 643-650.

J. H. Giovanola, R. W. Klopp, and T. Kobayashi, "Toughness and Fracture Mechanisms of Titanium-10V-2Fe-3Al Microstructures at High Loading Rates," in preparation. To be submitted to Metallurgical Transactions A.

J. H. Giovanola, R. W. Klopp, and J. W. Simons, "Dynamic Crack Propagation Studies in Titanium-10V-2Fe-3Al," in preparation. To be submitted to Engineering Fracture Mechanics.

PRESENTATIONS

D. C. Erlich and D. A. Shockey, "Instability Conditions for Cracks Under Short-Duration Pulse Loads," Topical Conference on Shock Waves in Condensed Matter, Meeting of the American Physical Society, Washington State University, Pullman, WA, June 11-13, 1979.

D. A. Shockey, "Instability Conditions for Cracks Loaded by Short Stress Pulses," Poulter Laboratory Seminar, SRI International, Menlo Park, CA, December 12, 1979.

D. A. Shockey, "Dynamic Crack Instability," Institut CERAC, Ecublens, Switzerland, May 19, 1980.

D. A. Shockey, "Dynamic Crack Instability," Institut für Werkstoffmechanik, Freiburg, Germany, May 21, 1980.

D. A. Shockey, "Simultaneous Measurements of Stress Intensity and Toughness for Fast Running Cracks in Steel," Poulter Laboratory Seminar, SRI International, Menlo Park, CA, June 1980.

D. A. Shockey, "Criterion for Crack Instability Under Short Pulse Loads," Fifth International Conference on Fracture (ICF5), Cannes, France, March 29-April 3, 1981.

D. A. Shockey, "Simultaneous Measurements of Stress Intensity and Toughness for Fast Running Cracks in Steel," 18th Annual Meeting of the Society for Engineering Science, Inc., Brown University, Providence, RI, September 2-4, 1981.

D. A. Shockey, "Short Pulse Fracture Mechanics," Seminar for the Department of Applied Mechanics, Stanford University, Stanford, CA, March 3, 1983, C. Steele, Chairman.

D. A. Shockey, "Short Pulse Fracture Mechanics," Poulter Laboratory Seminar, SRI International, Menlo Park, CA, April 11, 1983.

J. H. Giovanola, "Mechanics of Fracture Under Pulse Loads; Minimum Time Theory Revisited," Poulter Laboratory Seminar, SRI International, Menlo Park, CA, April 1984.

J. H. Giovanola, "Material Failures at High Strain Rates, " two lectures given at the Department of Materials Science and Engineering of Stanford University, May 1984.

J. H. Giovanola, "Material Failures at High Strain Rate," Materials Science and Engineering Graduate Seminar, University of California at Berkeley, Berkeley, CA, November 1984.

J. H. Giovanola, "Investigation and Analysis of the One-Point-Bend Impact Test," presented at the ASTM Seventeenth National Symposium on Fracture Mechanics, Albany, NY, August 7-9, 1984.

D. A. Shockey, D. R. Curran, and L. Seaman, "Fracture Under Impact Loads," presented at the International Conference on Dynamic Fracture Mechanics, San Antonio, November 7-9, 1984.

J. H. Giovanola,"The One-Point-Bend Test: Experiment and Analysis," Poulter Laboratory Seminar, SRI International, Menlo Park, CA, March 1985.

D. A. Shockey, J. F. Kalthoff, M. Homma, and J. H. Giovanola, "Recent Results in Short Pulse Fracture Mechanics," presented at the SEM Spring Meeting, Las Vegas, June 1985.

J. H. Giovanola, "Crack Initiation and Extension in Steel for Short Loading Times," presented at DYMAT International Conference on Mechanical and Physical Behavior of Materials under Dynamic Loading, Paris, September 2-5, 1985.

J. H. Giovanola: "Fracture at High Loading Rates," presented at the University of California at Berkeley short course Fracture and Fatigue: Approaches for Analysis and Control of Failure, June 1986.

J. H. Giovanola, "Fracture at High Loading Rates," invited lecture for graduate fracture mechanics course (ME 225) at the University of California at Berkeley, April 14, 1987.

D. A. Shockey, "Recent Progress in Dynamic Fracture Testing and Treatment" invited lecture, Impact 87, International Conference on Impact Loading and Dynamic Behaviour of Materials, Bremen, FRG, May 18-22, 1987.

J. H. Giovanola "Review of Recent Dynamic Fracture Research at SRI International," presented to the Fatigue and Fracture Branch of the David Taylor Naval Ship Research and Development Center, Annapolis, MD, June 3, 1988.

J. H. Giovanola, "Effect of Strain Rate and Microstructure on the Fracture Behavior of Ti-10V-2Fe-3Al," Poulter Laboratory Seminar, SRI International, November 1988.

J. H. Giovanola, "Effect of Strain Rate and Microstructure on the Fracture Behavior of Ti-10V-2Fe-3Al," 7th International Conference on Fracture, Houston, March 20-24, 1989.

REFERENCES

1. "Standard Test Method for Plane-Strain Fracture Toughness of Metallic Materials," E 399, *Annual Book of ASTM Standards*, Vol 03.01 (American Society for Testing and Materials, Philadelphia, 1984), p. 519-554.

2. M. F. Kanninen, P. C. Gehlen, C. R. Barnes, R. G. Hoagland, G. T. Hahn, and C. H. Popelar, "Dynamic Crack Propagation Under Impact Loading," *Nonlinear and Dynamic Fracture Mechanics*, N. Perrone and S. N. Atluri, Eds. (American Society of Mechanical Engineers, New York, 1979), pp. 185-200.

3. J. F. Kalthoff, S. Winkler, W. Böhme, and D. A. Shockey, "Mechanical Response of Cracks to Impact Loading," in *Proceedings of the International Conference on Dynamical Properties and Fracture Dynamics of Engineering Materials* (Czechoslovak Academy of Sciences, Institute of Physical Metallurgy, Brno, Czechoslovakia, June 1983).

4. J. H. Giovanola and D. A. Shockey, "Dynamic Fracture Behavior of Structural Materials," SRI Final Report prepared for Air Force Office of Scientific Research, Contract No. AFOSR/F49620-81-K-0007, July 1986.

5. J. H. Giovanola, "Investigation and Application of the One-Point-Bend Impact Test," in *Fracture Mechanics: Seventeenth Volume, ASTM STP 905*, J. G. Underwood, R. Chait, C. W. Smith, D. P. Wilhelm, W. A. Andrews, and J. Newman, Eds. (American Society for Testing and Materials, Philadelphia, 1986), pp. 307-328.

6. J. H. Giovanola, "The One-Point-Bend Test," in *ASM Metals Handbook, 9th Edition, Volume 8, Mechanical Testing* (American Society for Metals, Metals Park, OH, 1985), pp. 271-275.

7. T. Nakamura, C. F. Shih, and L. B. Freund, "Analysis of a Dynamically Loaded Three-Point-Bend Ductile Fracture Specimen," Brown University Report ONR0365/1 (1985).

8. T. Kobayashi and D. A. Shockey, "Fractographic Investigation of Thermal Embrittlement in Cast Duplex Stainless Steel, " Metall. Trans. **18A**, 1941-1949 (1987).

9. G. T. Terlinde, T. W. Duerig, and J. C. Williams, "Microstructure, Tensile Deformation, and Fracture in Aged Ti-10V-2Fe-3Al," Metall. Trans., **14A**, 2101-2115 (1983).

10. G. Terlinde, H. J. Rahjen, and K. H. Schwalbe, "Microstructure and Fracture Toughness of the Aged β-Ti Alloy Ti-10V-2Fe-3Al," Met. Trans., **19A**, 1037-1049 (1988).

11. D. R. Curran, L. Seaman, and D. A. Shockey, "Dynamic Failure of Solids," Physics Reports, Vol. 147, Nos. 5 & 6 (March 1987).